Gallery of Fluid Motion

Visualization and feature tracking of the atomization of impinging jets

Evan Pruitt, William Markiewicz, Carlos Gonzalez, and Xiaofeng Liu *
Department of Aerospace Engineering, San Diego State University, San Diego, California 92182, USA

(Received 4 June 2024; published 22 November 2024)

This paper is associated with a video winner of a 2023 American Physical Society's Division of Fluids Dynamics (DFD) Gallery of Fluid Motion Award for work presented at the DFD Gallery of Fluid Motion. The original video is available online at the Gallery of Fluid Motion, https://doi.org/10.1103/APS.DFD.2023.GFM.V0019

DOI: 10.1103/PhysRevFluids.9.110513

Impinging jet injectors are useful atomization devices for mixing and atomization of liquid fuels and oxidizers. This has particular applications to rocket engines to ensure efficient and stable combustion of liquid propellants. Most famously, impinging jet injectors were used in the F-1 engines that powered the first stage of the Saturn V rocket [1]. Additionally, impinging jet injectors have been used in the manufacture of nanoparticles [2] and the delivery of aerosol medication [3]. It is therefore highly desirable to increase our understanding of the phenomenon and to better explore the dynamics at play. Here we present a method that enhances our ability to design effective injectors by experimentally characterizing the spray atomization process in greater detail than previously possible. This method is henceforth referred to as atomization feature identification tracking and analysis or AFITA.

Figure 1 illustrates the two-phase flow phenomenon that the impinging jet injector creates where atomization is achieved through wave instabilities inherent in a liquid sheet that is formed as a result of the liquid jet impingement [4]. Previous work has been done to examine the different elements of the atomization process such as liquid sheet surface features tracking [5], particle and ligament tracking [6], and nonintrusive droplet size measurement [7–9]. However, no previously developed tool is able analyze all the major atomization features simultaneously to capture the entire process in a time resolved manner. AFITA is an integrated method for identifying, tracking, and analyzing the liquid sheet, the attached ligaments, the detached ligaments, and droplets during the entire atomization process.

In the schematic of the injector along with a model of the spray shown in Fig. 1, the doublet injector has an outlet diameter of $d_j = 3.0$ mm, an impingement angle $2\alpha = 60^\circ$, and a distance from the jet nozzle exit to the impingement point of 26.42 mm. In this experiment, water is used as a simulant for propellant atomization, and the flow speed through the nozzles is $u_j = 5.7$ m/s. The primary characteristic dimensionless numbers for the experiment are the Reynolds number (Re = 18 000), the Weber number (We = 1300), and the Ohnesorge number (Oh = 0.0020). These

*Contact author: Xiaofeng.Liu@sdsu.edu

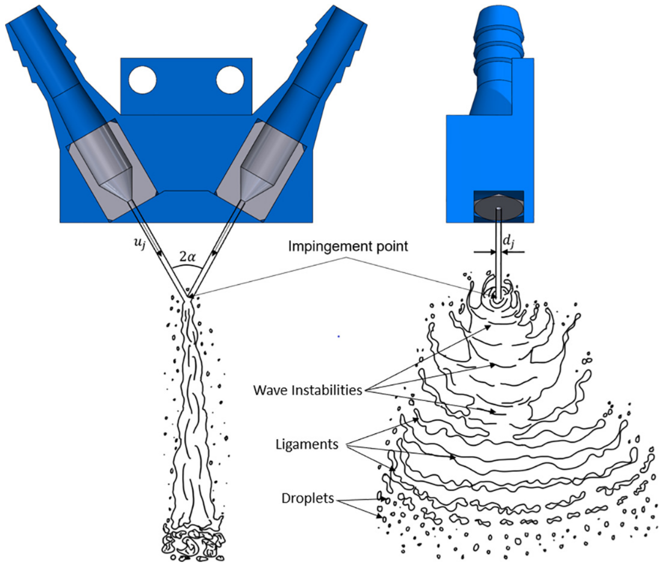

FIG. 1. Diagram of impinging jet atomization.

dimensionless parameters are defined as $\mathrm{Re} = \frac{\rho u_j d_j}{\mu}$, $\mathrm{We} = \frac{\rho u_j^2 d_j}{\sigma}$, and $\mathrm{Oh} = \frac{\mu}{\sqrt{\rho \sigma d_j}} = \frac{\sqrt{\mathrm{We}}}{\mathrm{Re}}$, where ρ is the density, μ the dynamic viscosity, and σ the surface tension of the water.

Images of the spray were captured in the orientation shown on the right side of Fig. 1. This gives a quasiplanar field of view for the atomization process as the displacements of the sheet toward and away from the camera are relatively small. The camera used for image acquisition is a Photron FastCAM SA-Z high speed camera. Images were acquired at a rate of 20 000 fps with a shutter speed of 1/100 000 s to minimize blur. At this frame rate, it was possible to acquire 1024×1024 pixel images which corresponded to a 46.2 mm×46.2 mm field of view at a physical length to pixel conversion scale of 45.1 μm per pixel.

The method for detecting major components of the atomization process is illustrated in Fig. 2. The procedure begins by taking the original image, Fig. 2(a), and applying an adaptive Gaussian threshold to create Fig. 2(b) [10]. This thresholding allows delineation of all of the edges in the image including those of the sheet, ligaments, and droplets. Using proper definitions for each of the different components, e.g., the liquid sheet is the largest contour and contains the impingement point, each atomization element is identified. Figure 2(c) shows the outline of different features represented by different gray scale values. In this figure, dark gray identifies the primary liquid sheet, light gray identifies both the attached and detached ligaments, and white identifies the droplets. The features are highlighted using an overlay of different colors in Fig. 2(d), in which the background is unchanged, with the primary liquid sheet being dyed in cyan, the ligaments in dark red, and the droplets in light red.

Once the droplets and ligaments are identified, AFITA will then track these components as they move through the field of view. An example of the tracking is shown in Fig. 3. The bounding boxes that are obtained from a component identification step are highlighted in Fig. 3(a). These bounding boxes were fed into the discriminative correlation filter with channel and spatial seliability (DCF-CSR) tracker [11] that is provided in the OpenCV library [12]. A subset of tracked paths can be seen in Fig. 3(b). In this figure, each tracked droplet is given a unique color so as to be identified. The droplets are outlined by their respective bounding boxes. The pathlines of droplets are also shown for a course of 20 frames prior to the current instant of time. This gives a visual representation of the trajectories that the droplets are taking and how they radiate from the center of

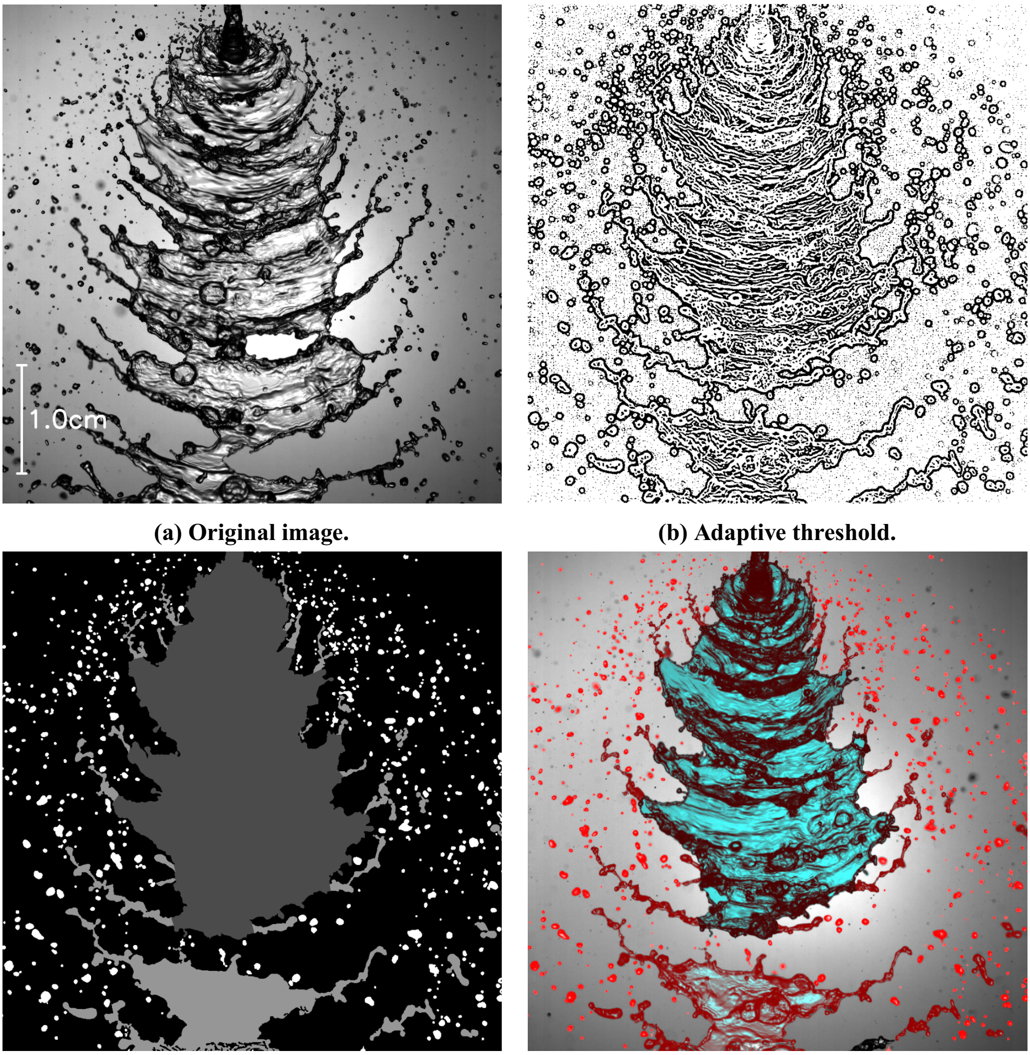

(a) Original image. (b) Adaptive threshold. (c) Identification of components and labeling. (d) Components highlighted in original image.

FIG. 2. Visual algorithm for atomization component detection. The images are adapted still frames from the GFM video entry at Ref. [13].

the jet impingement. With the time history of the particle trajectories available, the histories of the droplet velocity and the acceleration variations along with its motion are then inferred.

Finally, AFITA characterizes the waves on the liquid sheet that cause the atomization to take place. The primary characteristics of a traveling wave are the wavelength, frequency, speed, and amplitude. Here we demonstrate a method for measuring the wavelength λ and frequency f of the dominant waves on the sheet. From the values of λ and f we can then calculate the speed of these waves using the relation $u_{\mathrm{wave}} = f\lambda$, thus giving all of the primary information about the large waves with the exception of the amplitude.

The wavelength of the dominant waves are determined by performing spectral analysis of a narrow rectangular sample area within the sheet flow field, as shown in Fig. 4(a). First a rectangular sample area is selected, which is outlined in red in the original image. The image gray-scale intensity

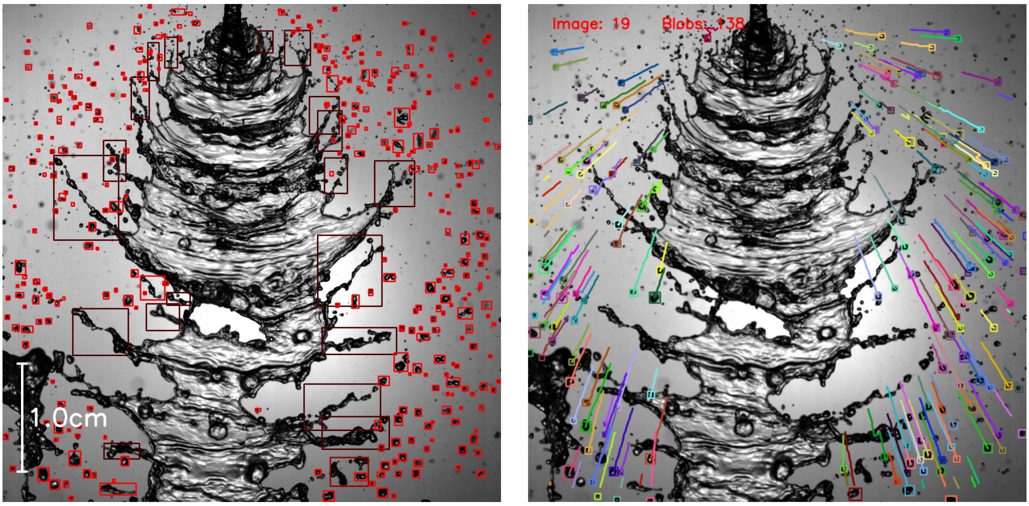

(a) Bounding boxes for tracked objects based on the initial detection step.

(b) Example of tracked droplet paths over a course of 20 frames prior to the current instant of time.

FIG. 3. Object tracking example showing the bounding boxes and trajectories of different atomization components. The image shown in (a) is an adapted still frame from the GFM video entry at Ref. [13].

in the sample area will then be averaged along each horizontal band to reduce noise and reveal the dominant wave structure. Spectral analysis is then performed on the horizontally averaged sample area which reveals the spectroscopic wavenumber space. The peak spectroscopic wavenumber are then extracted and converted to a wavelength. This analysis is performed across all images and an average peak wavenumber and associated wavelength can be determined for the entire set of image recording.

Two different methods were used to determine the frequency of the waves which both used the averaged intensity of a small square sample area, as shown in Fig. 4(b). The first was to perform spectral analysis in the frequency domain using the average light intensity over the sample area throughout time. The second was to use a pulse counting method where a wave was detected whenever the average light intensity of the sample area dropped below a low threshold after having been above a high threshold. The low threshold represents a dark region when a wavefront is passing by and the high threshold represents when there is no wavefront appearing. Please note that the sample square box has a side length smaller than the width of the dominant wave bands. In the

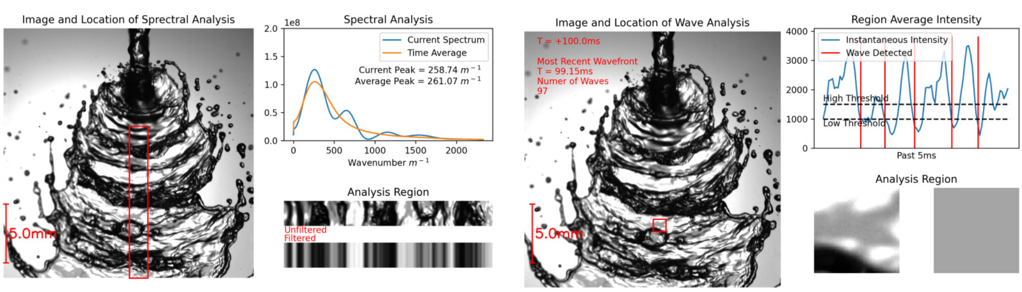

(a) Spectral analysis for wavenumber determination.

(b) Spectral analysis for wave frequency determination.

FIG. 4. Determination of the impact wave characteristics of the impinging jet. The images are adapted still frames from the GFM video entry at Ref. [13].

bottom right of the figure, a magnified version of the sample area is shown, as is the average light intensity within the area. In the top right, a plot of the area's average image intensity is plotted for a 5 ms duration of sampling, with red lines showing the time when wavefronts were detected.

Through the use of AFITA, we demonstrate the ability to gain greater insight into the atomization process of impinging jet than was previously possible. This enhanced insight makes it possible to test and design injectors with precise characteristics that can enhance combustion in rocket engines, better control the manufacturing of nanoparticles, and better deliver medication. Future studies should be done that utilize this method in both the design process as well as to build out a more thorough scientific understanding of the mechanisms in the atomization process.

The U.S. DoD equipment fund (Award No. W911NF2110158) and the San Diego State University Student Success Fee Program support are gratefully acknowledged. Evan Pruitt thanks the San Diego State University for the 2023 Master's Research Scholarship support.

---

[1] J. C. Oefelein and V. Yang, Comprehensive review of liquid-propellant combustion instabilities in F-1 engines, J. Propul. Power **9**, 657 (1993).

[2] O. Proskurina, R. Abiev, D. Danilovich, V. Panchuk, V. Semenov, V. Nevedomsky, and V. Gusarov, Formation of nanocrystalline $BiFeO_3$ during heat treatment of hydroxides co-precipitated in an impinging-jets microreactor, Chem. Eng. Process. Process Intensif. **143**, 107598 (2019).

[3] H. Wachtel, Respiratory drug delivery, in *Microsystems for Pharmatechnology*, edited by A. Dietzel (Springer International Publishing, Cham, 2016), pp. 257–274, https://link.springer.com/chapter/10.1007/978-3-319-26920-7_9.

[4] R. J. Santoro, W. E. Anderson, and M. R. Harry, III, Impact wave-based model of impinging jet atomization, Atomization and Sprays **16**, 791 (2006).

[5] K. S. Siddharth, M. V. Panchagnula, and T. J. Tharakan, Feature correlation velocimetry for measuring instantaneous liquid sheet velocity, J. Fluids Eng. **139**, 091401 (2017).

[6] K. Warncke, S. Gepperth, B. Sauer, A. Sadiki, J. Janicka, R. Koch, and H. J. Bauer, Experimental and numerical investigation of the primary breakup of an airblasted liquid sheet, Int. J. Multiphase Flow **91**, 208 (2017).

[7] J. B. Blaisot and J. Yon, Droplet size and morphology characterization for dense sprays by image processing: Application to the Diesel spray, Exp. Fluids **39**, 977 (2005).

[8] S. V. Minov, F. Cointault, J. Vangeyte, J. G. Pieters, and D. Nuyttens, Spray droplet characterization from a single nozzle by high speed image analysis using an in-Focus droplet criterion, Sensors **16**, 218 (2016).

[9] A. Asgarian, Z. Yang, Z. Tang, M. Bussmann, and K. Chattopadhyay, An image feature consolidation technique (IFCT) to capture multi-range droplet size distributions in atomizing liquid sheets, Exp. Fluids **61**, 14 (2020).

[10] B. Gatos, I. Pratikakis, and S. J. Perantonis, Adaptive degraded document image binarization, Pattern Recognit. **39**, 317 (2006).

[11] A. Lukezic, T. Vojir, L. Cehovin Zajc, J. Matas, and M. Kristan, Discriminative correlation filter with channel and spatial reliability, in *Proceedings of the IEEE Conference on Computer Vision and Pattern Recognition (CVPR)* (IEEE, Piscataway, NJ, 2017).

[12] G. Bradski, The OpenCV Library, *Dr. Dobb's Journal of Software Tools*, 2000.

[13] https://doi.org/10.1103/APS.DFD.2023.GFM.V0019.